Modeling high-order plasmon resonances of a U-shaped nanowire used to build a negative-index metamaterial

Francisco J. Rodríguez-Fortuño,* Carlos García-Meca, Rubén Ortuño, Javier Martí, and Alejandro Martínez
Valencia Nanophotonics Technology Center, Universidad Politécnica de Valencia, Campus del Camino de Vera, 46022 Valencia, Spain
(Received 3 September 2008; published 6 February 2009)

We apply the concept of slow surface-plasmon polariton standing-wave resonances to model the plasmon resonances which exist on split-ring resonators (U-shaped nanowires) forming the unit cell of a metamaterial at infrared frequencies. We compare the expected resonances predicted by the model with full electrodynamic three-dimensional simulations of the U-shaped nanowires for varying geometrical parameters and find a reasonably good agreement. We also consider how far-field dipolar coupling between unit-cells and near-field coupling between the U-shaped nanowire's arms should be taken into account. In addition, we study how the different resonances give rise to negative constitutive parameters for the metamaterial and adjust the geometrical parameters so that the second and third order slow-SPP standing-wave resonances of the U-shaped nanowires result in a double-negative behavior at far-infrared wavelengths without the need of further wires or particles. Finally, we study the effects of stacking N layers of such metamaterial, where each resonant mode splits into N normal mode resonances, showing different electric or magnetic responses. This simple stacked structure maintains the left-handed behavior, exhibiting backward wave propagation.

DOI: 10.1103/PhysRevB.79.075103 PACS number(s): 41.20.Jb, 73.20.Mf, 71.45.Gm, 81.05.Bx

I. INTRODUCTION

Artificially structured materials, termed metamaterials, are composed of artificial atoms much smaller than the wavelength of the incident electromagnetic field, which allow the metamaterial to be modeled by an effective homogenous medium to which constitutive electromagnetic parameters ε_{eff} and μ_{eff} can de ascribed. Of particular interest are the so-called left-handed metamaterials (LHM) showing a negative index of refraction which can be produced by a negative electric permittivity ε_{eff} and a negative magnetic permeability μ_{eff} at the same frequency.[1] These LHMs show unusual optical properties and have the potential application of a perfect lens.[2]

The negative permeability $\text{Re}(\mu_{\text{eff}})<0$ is typically achieved at microwave frequencies by using split ring resonators (SRRs).[3] Considerable effort was done to scale down the SRRs to terahertz, telecommunication, and optical frequencies[4,5] which required advanced lithography techniques (other methods for achieving negative permeability at optical frequencies with less elaborate shapes include the use of spherical semiconductor[6] or metallic[7] particles). At high frequencies, the *LC* model of the SRR, valid at microwave frequencies, had to be refined.[8] Finally, the *LC* resonance at optical frequencies was reinterpreted as a surface-plasmon polariton (SPP) resonance.[9,10] This gave much physical insight into the various resonances observed in SRRs at optical frequencies, which were all identified as higher order plasmon resonances.

The so-called surface-plasmon polaritons are propagating electromagnetic waves sustained along a metal/dielectric interface, coupled to collective oscillations of the conduction electrons in the metal.[11] These waves propagate highly confined to the interface, with the fields exponentially decaying away from it.

In particular, a metallic nanowire at optical frequencies allows propagation of leaky and bound SPP waves along its length.[12–14] One of the bound modes supported by nanowires is the short ranging surface-plasmon polariton (SR-SPP), also called slow SPP, which is highly confined inside the metal, thereby slowing down the mode propagation while increasing the attenuation. If we consider metallic nanowires finite in length, one can model the end faces as reflecting the incident SR-SPP modes (but not the other modes, namely, the long ranging SPPs, which show weak reflection at the ends)[15,16] and turn the nanowire into a resonator[15–20] showing standing slow-SPP waves when the nanowire length is approximately an integer of the half of the plasmon wavelength.

These slow-SPP standing-wave resonances have been identified in optical nanoantennas,[19] and can play a role in the building blocks of metamaterials at optical frequencies.[21] In Ref. 9 the resonances of a SRR where associated with plasmon resonances: we bring this interpretation one step further by explicitly applying the slow-SPP standing-wave nanowire resonator model to the SRR resonances. We also carry out a numerical study on the possibility of using the usually overlooked higher order slow plasmon resonances of the SRR (in particular the second and third order) to achieve electric and magnetic polarizability, and thus negative constitutive parameters. This way we obtain a double-negative metamaterial at far-infrared frequencies with a single element in the unit cell (SRRs alone), unlike most metamaterial designs which (with some exceptions[22,23]) require further wires or particles.

II. ANALYZED STRUCTURE AND NUMERICAL TOOLS

A single unit cell of the analyzed metamaterial consists of a gold U-shaped nanowire as shown in Fig. 1, which depicts the relevant geometrical parameters. The nanowire lies in the *XZ* plane and the unit cell is repeated in the x and y directions with a_x and a_y periodicity, respectively.

Three-dimensional numerical calculations were per-

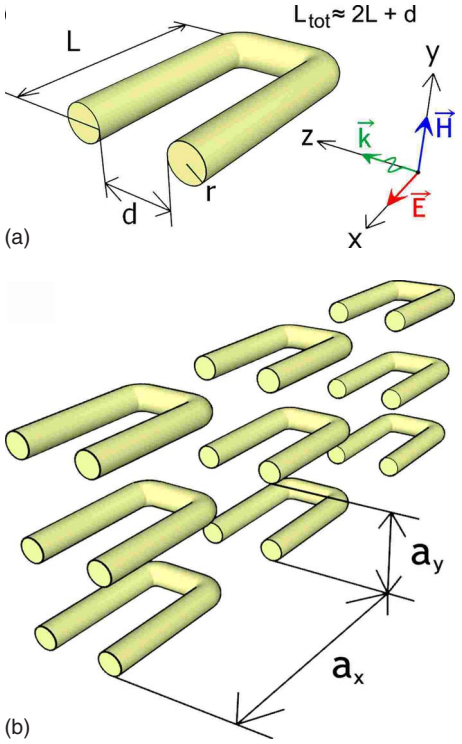

FIG. 1. (Color online) (a) Unit cell of the analyzed metamaterial showing the relevant geometrical parameters and the incident plane wave. (b) Single layer metamaterial used in simulations.

formed using a commercial electromagnetic solver (CST MICROWAVE STUDIO). A plane wave propagating in the z direction with the magnetic field parallel to the y axis (perpendicular to the nanostrip plane) was incident in the structure, and the transmission and reflection coefficients were obtained for a certain frequency range. Field patterns and electric currents inside the nanostrip at certain frequencies were also obtained.

For our simulations, gold's permittivity was modeled using the Drude model $\varepsilon(\omega)=\varepsilon_\infty-\omega_p^2/(\omega^2+i\gamma\omega)$, where $\varepsilon_\infty=9$, $\omega_p=1.3673\times10^{16}$ rad/s is the plasma frequency, $\gamma=1/\tau=1.0027\times10^{14}$ s^{-1} is the collision frequency and $\omega=2\pi c/\lambda$. At far-infrared frequencies, gold's permittivity is in the free-electron region, so the Drude model fits very well to experimental data.[24] Later in the paper, an unrealistic value for the collision frequency of $\gamma=1\times10^{12}$ s^{-1} was used to provide better insight into the resonances.

III. MODEL OF SLOW-PLASMON STANDING-WAVE RESONANCES

A. Analytical model for surface plasmons in a straight finite length nanowire

Throughout this paper, we modeled a cylindrical nanowire as a standing-wave slow-SPP resonator.[15–20] To calculate the expected frequencies at which the mth order resonance will occur, we used the standing-wave condition:[15]

$$\beta_{SPP}L_{tot}=m\pi-\varphi, \tag{1}$$

where $\beta_{SPP}(\omega)=2\pi/\lambda_{SPP}(\omega)=k_0n_{SPP}(\omega)=(\omega/c)n_{SPP}(\omega)$ is the propagation constant of the SPP, L_{tot} is the total length of the nanowire, m is an integer, and φ is the phase shift due to reflection of the SPP mode at the wire ends. For simplicity we consider $\varphi=0$, which is equivalent to modeling the nanowire ends as perfect magnetic walls.

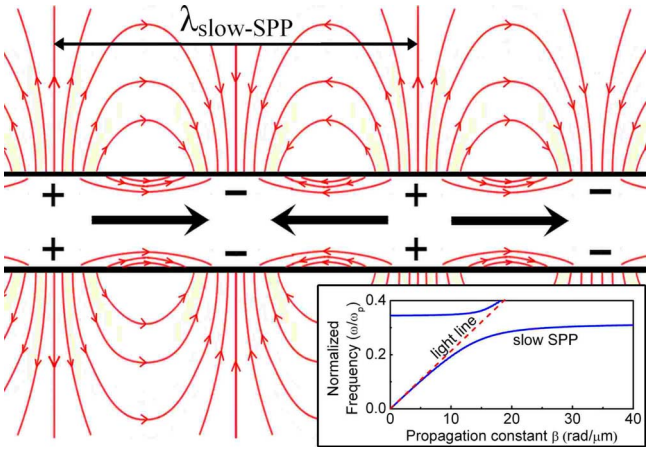

FIG. 2. (Color online) Analytically calculated field at a certain instant for a slow-SPP standing-wave resonance on an infinite cylindrical nanowire of radius 100 nm. Thin red lines represent the electric field lines. The magnetic field (not shown) circles around the nanowire. Thick black lines represent the direction of current flow. The + and − signs represent the charge accumulation along the nanowire. Inset: calculated dispersion relation of the slow-SPP mode.

To obtain the resonance frequencies from the resonance condition, we need the dispersion relation $\beta_{SPP}(\omega)$ of the slow SPP on a cylindrical nanowire. Such slow SPP corresponds to the first-order bound mode supported by the infinite cylinder, in which all fields show invariance with the angle in cylindrical coordinates θ (specifically this implies $n=0$ where the fields are multiplied by a harmonic term $e^{in\theta}$). The dispersion relation of the slow-SPP mode is given by[12–14]

$$\frac{\gamma_m I_1(\gamma_d r)K_0(\gamma_m r)}{\gamma_d I_0(\gamma_m r)K_1(\gamma_d r)}=-\frac{\varepsilon_d}{\varepsilon_m} \tag{2}$$

$$\gamma_i=\sqrt{\beta_{slow\text{-}SPP}^2-\varepsilon_i\mu_0\omega^2}\quad i=d,m,$$

where ε_d is the permittivity of the surrounding dielectric, ε_m is the metal permittivity following the Drude model, and r is the radius of the nanowire. The calculated real part of $\beta_{slow\text{-}SPP}(\omega)$ using the dispersion relation is shown in the inset of Fig. 2.

Equations (1) and (2) yield the frequencies at which an incident excitation with the appropriate symmetry conditions can couple to the standing-wave slow-SPP resonances. At these frequencies, dips in the transmission spectra will be seen. The inverse procedure can also be done:[25] experimentally observing the extinction peaks in the spectra of transmission through arrays of nanofabricated finite length nanowires can be used to experimentally deduce the dispersion relation $\beta_{slow\text{-}SPP}(\omega)$.

The analytical field distribution[14] of these slow-SPP standing waves is plotted in Fig. 2. The electric field is symmetrical with respect to the cylinder axis, and all fields show invariance with the angle in cylindrical coordinates θ. If one looks at the electric field inside the metal nanowire, it can be seen that it consists of consecutive half-λ_{SPP} sections with the longitudinal electric field component oriented toward alternating directions (in fact showing a sinusoidal variation with period λ_{SPP} along the propagation direction). The current inside the metal nanowire will be proportional to the electric field and therefore will follow the same alternating pattern.

To check the model, we simulated a plane-wave incident into an array of gold nanowires, with the electric field parallel to the nanowire axis. The odd mth order slow-SPP standing-wave resonances were clearly identified as extinction peaks in the transmission spectrum (the even mth order resonances were not observed since they cannot be excited by the incident electric field due to symmetry considerations). The field and current distributions showed strong resemblance to Fig. 2 except near the nanowire ends. The frequency of the first and second resonances showed a good agreement with the model, while the third resonance happened lower in frequency than expected. A similar shift was observed experimentally at high frequencies in Ref. 25 and it is suggested in Ref. 15 that this shift could be due to not considering a phase change φ upon reflection at the ends.

B. Resonator model for surface plasmons on a U-shaped nanowire

To completely characterize the SPP resonances on a U-shaped nanowire, one should solve the full electrodynamic Maxwell equations on the particular geometry. However, it would be useful to have at our disposal a simpler model to predict the resonant frequencies and field distributions, as well as their dependence with geometrical parameters. It is reasonable to associate the resonances on a U-shaped nanowire to the corresponding resonances on a straight nanowire of same total length as modeled above, although some inaccuracies arise from this process. The definition of the total length L_{tot} becomes ambiguous: we defined the total length of the nanowire as the length along its center, but the electric currents predominantly occur near the surfaces of the cylinder. Also the model does not take into account possible couplings between the propagating SPPs, especially at the bends of the U-shaped nanowire, and it is known that SPP propagation along curved metal surfaces increases the attenuation and modifies the phase.[26]

C. Current and field configurations yielding negative parameters

Knowledge of the currents inside a finite length nanowire at each resonance (showing sinusoidal variation along its length) allowed us to predict the currents in the equivalent U-shaped nanowire. Just above the resonant frequency, these currents are known to lag behind the driving electromagnetic fields, thus creating either electric or magnetic dipolar moments which can be parallel and opposed to the incident

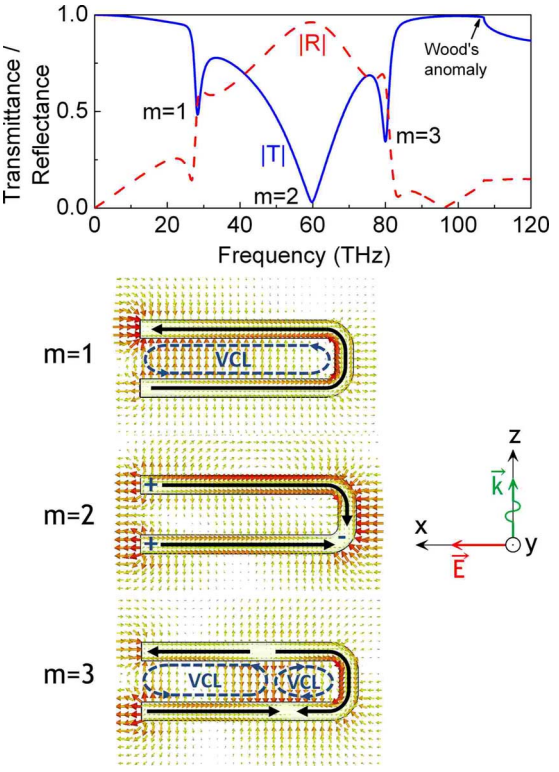

FIG. 3. (Color online) Transmittance and reflectance spectra of the analyzed metamaterial upon plane-wave excitation as shown in Fig. 1. Geometrical parameters are: r=100 nm, d=450 nm, L=2125 nm, L_{tot}=4700 nm, a_x=a_y=2800 nm. The three first resonances are seen as dips in the spectrum and the simulated electric field distribution is shown for a particular instant in each resonance. Thick arrows indicate the current flow. Discontinuous arrows indicate the VCLs (electric current loops closed by displacement fields).

electric or magnetic field. When the U-shaped nanowires are sufficiently small compared to the wavelength, they can act as the unit cell of a homogenous metamaterial medium which then shows a Lorentz-type response in the effective permittivity or permeability, respectively. If this response is strong enough it can result in negative constitutive parameters.

We simulated some examples of bent nanowire plasmon resonances leading to virtual current loops (VCL) and thus a Lorentz-type response on the magnetic permeability μ_{eff},[27] such as the first-order resonance on a U-shaped nanowire (the well-known LC resonance discussed below) and the second-order resonance on an S-shaped nanowire (not shown).

IV. NUMERICAL RESULTS

A. Resonances on a U-shaped nanowire

We interpret the resonances that appear in a U-shaped nanowire at optical frequencies as slow-SPP standing-wave resonances. Figure 3 shows the simulated transmission and reflection spectra of a metamaterial composed of U-shaped nanowires (geometry as shown in Fig. 1), and the corresponding electric field and current distributions for each

resonance. The geometrical dimensions used are $L=2125$ nm, $d=450$ nm, $r=100$ nm, and $a_x=a_y=2800$ nm. Results agree qualitatively with those in Ref. 10. As it can be seen, the current distributions in each mode labeled m show m different sections of the nanowire with the current oriented at alternating directions. These current distributions agree with the known analytical currents shown in Fig. 2 for the slow-SPP standing-wave resonances if the straight nanowire was bent into a U shape. Also the electric and magnetic fields show the patterns that would intuitively arise from bending a finite straight nanowire. We believe that this field and current coincidence strongly supports the adequacy of the standing-wave resonator model for the U-shaped nanowire.

The first resonance is the so-called *LC* resonance of the SRR, and can be interpreted as the first plasmonic standing wave of the equivalent straight nanowire, (when $\lambda_{\text{slow-SPP}}=2L_{\text{tot}}$). The virtual current loop (electric current closed by an electric displacement field) seen around all the structure and perpendicular to the incident magnetic field is responsible for a magnetic Lorentz-type response. On the other hand, the net electric dipolar moment shown by the charge distributions is small and oriented only in the z direction, so, as we will see, the electric response and the dipolar far-field interaction between unit cells are weak on this first resonance.

The second resonance is usually called Mie resonance or electric plasmon resonance, and corresponds to the second plasmonic standing-wave resonance of the equivalent nanowire (when $\lambda_{\text{slow-SPP}}=L_{\text{tot}}$). The charge distribution shows a clear net electric-dipole moment in the x direction (parallel to the incident electric field) and so this resonance shows a Lorentz-type electric response, which can yield a negative permittivity. Also, due to the net electric-dipole moment, the position and strength of this resonance highly depends on the far-field dipolar interaction between unit cells.

The third resonance corresponds to the third plasmonic standing-wave resonance of the equivalent nanowire. It can be seen that two opposing virtual current loops are created but one of them has a greater area and thus dominates, which together with the electric quadrupole[28] observed in the charge distribution gives this resonance a magnetic Lorentz-type response. It is this third resonance that we will use together with the second one to attain a negative refractive index. Its high frequency in comparison with lower order resonances makes it particularly sensible to a damping of the resonance due to a high electron mass inductance[8] as compared to the geometrical inductance, so special care must be taken for this resonance to be strong enough as to show a negative real part of the permeability.

Above the third resonance, the well-known Wood anomaly appears where expected,[29,30] corresponding to the frequency in which the first grating order changes from evanescent into propagating at grazing angle. The following higher order resonances occur above the Wood anomaly, where the first grating order is propagating, and so are affected by great damping due to radiative losses.

We applied the effective parameter retrieval method[31–33] using the simulated transmission and reflection spectra. The retrieved ε_{eff} and μ_{eff} are shown in Fig. 4 and correspond only to propagation along z direction and for the polarization shown in Fig. 1. The homogeneous medium equivalence is poorly justified given that the unit cell's size in the propagation direction is only just below $\lambda/4$ for the third resonance, however the results agree with expectations. The Lorentz-type resonances are clearly seen for μ_{eff} at the first and third resonance, and for ε_{eff} at the second resonance. The corresponding antiresonance in the other parameter due to a finite wave vector[34] can also be seen in each case.

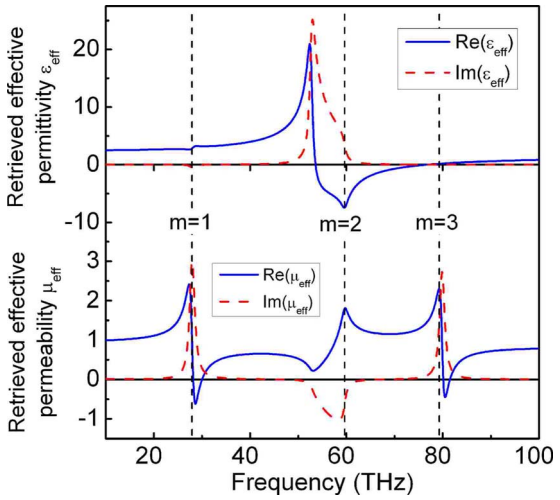

FIG. 4. (Color online) Retrieved electromagnetic parameters from the simulated transmittance and reflectance spectra of Fig. 3. For the retrieval procedure, the equivalent metamaterial slab thickness was adjusted to the limits of the metal. The frequencies of the first three standing-wave resonances are indicated with dashed lines.

In order to obtain a double-negative metamaterial, our aim was to push the second and third resonances closer, so that the negative permeability achieved by the third resonance occurred on the frequency range after the second resonance at which permittivity is seen to be negative. To achieve this we performed several simulations to deduce the dependence of the resonances with the geometrical parameters.

B. Resonance shifts through changes on geometrical parameters

1. Changes in the nanowire length

We define the total length of the nanowire L_{tot} as the longitudinal length measured through its center, which is approximately given by $L_{\text{tot}}=2L+d$. By varying the total length we change the standing-wave condition [Eq. (1)] so shifts in the resonances occur as seen in Fig. 5(a). At frequencies $\omega \ll \omega_p$ and large nanowire radii (compared with the penetration depth), the dispersion relation for the SR-SPP follows the light line very closely, so the expected resonance wavelengths accurately fall on $L_{\text{tot}}=n\lambda/2$ as in classical RF dipole antennas.

The third-order resonance is always seen lower in frequency than the model prediction. This difference probably arises from a frequency-dependent phase change φ upon reflection of the slow-SPP at the nanowire ends,[15] taken to be zero in our model.

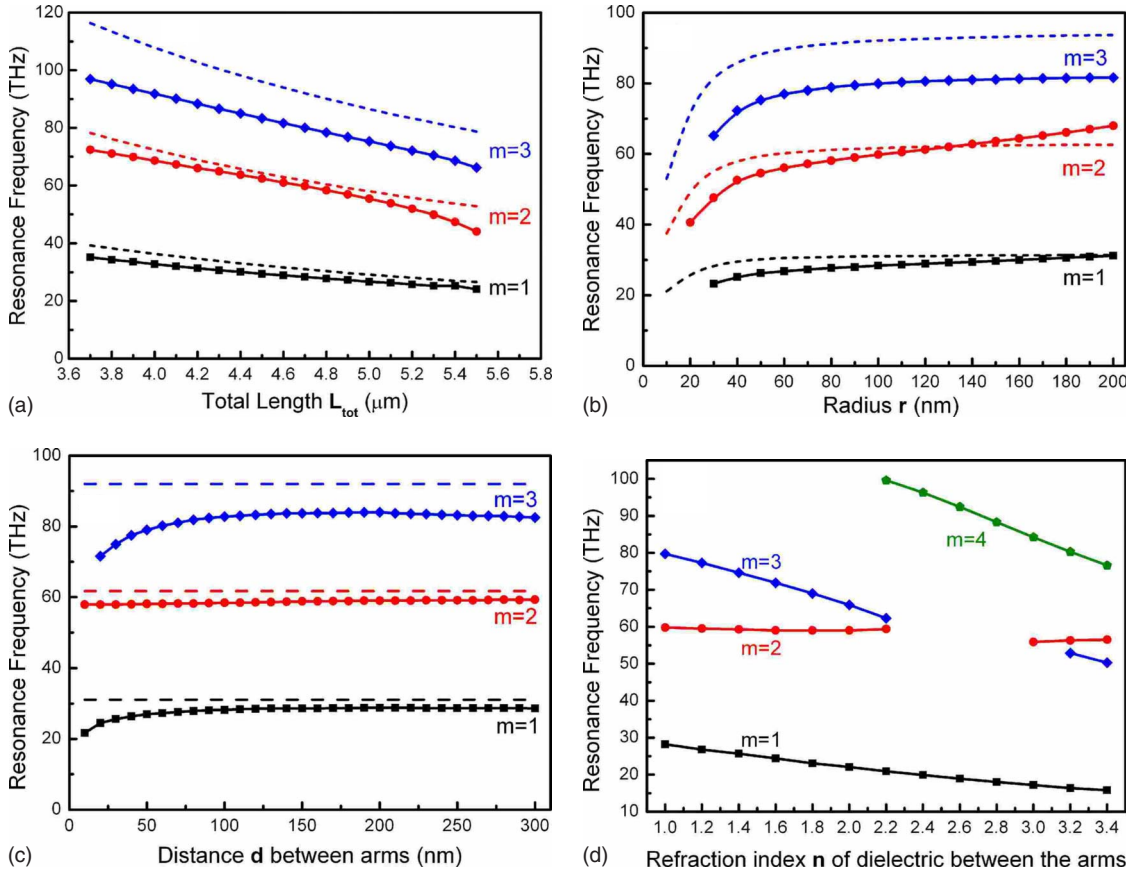

FIG. 5. (Color online) Resonant frequency of the first standing-wave modes of the metamaterial shown in Fig. 1 with varying (a) total length, (b) nanowire radius, (c) distance between arms, and (d) index of refraction of a dielectric inserted between the arms. The other geometrical parameters are kept constant to the values indicated in Fig. 3. The solid lines show the results from our simulations, while the dashed lines in (a) to (c) show the results calculated from the slow-SPP standing-wave resonator model using Eqs. (1) and (2). When two resonances cross in frequency and form a single dip, no line is plotted because the two resonances cannot be resolved.

2. *Changes in the nanowire radius* (*r*)

The dependence of the resonance frequency as a function of the nanowire radius is shown in Fig. 5(b). In accordance with the theoretical model, the slow-SPP modes are lowered in frequency when the radius of the nanowire is reduced below the penetration depth, which also increases the losses of the slow SPP, as determined by the imaginary part of $\beta_{\text{slow-SPP}}(\omega)$ from the dispersion relation in Eq. (2).

3. *Changes in the distance between arms* (*d*)

In Fig. 5(c) we plot the resonant peak dependence with the separation between the two arms of the U-shaped nanowire. For a fair comparison, the total length of the nanowire L_{tot} was set constant, so we decreased the arm length L as d was increased. Our slow-SPP nanowire resonator model considers a straight nanowire and so cannot take into account distance between arms, so the model resonant frequencies in the graph are constant.

It can be seen that for small distances, the odd modes (which show opposite current flow on the two arms) shift down in frequency. We interpret this as a coupling effect: the electric field created by the SPP on one arm opposes the electric current flow of the SPP on the other, thus increasing the restoring force of the electron oscillations, which leads to a redshift in the resonances. A weakening of the magnetic response is also observed due to the reduction in the area of the VCLs (in fact, for decreasing values of d less than 20 nm, the odd resonances are seen to gradually disappear).

The second mode is not affected by the strong redshift nor weakened, as both arms have the current flowing in the same direction and no increased restoring force occurs. In fact, when $d \rightarrow 0$ the second mode coincides with the first mode of a straight nanowire of length L (instead of L_{tot}).

The coupling behavior of the odd modes agrees qualitatively with an analytical model for the magnetic plasmon resonance (MPR) (Ref. 35) on two contiguous nanowires, which on Ref. 35 is studied on the same first resonance of a U-shaped nanowire which we study here. Unfortunately, applying the MPR formula to plot the expected resonant frequency in this case was not suitable, as the condition $L \gg d \gg 2r$ used in Ref. 35 does not hold in our structure. The MPR is accurate for very thin nanowires (thinner than a skin depth) where the slow-SPP mode is heavily confined inside the metal and slowed down, which enables a "squeezed" resonance with a total length much smaller than the free-space wavelength, at the expense of greater damping.

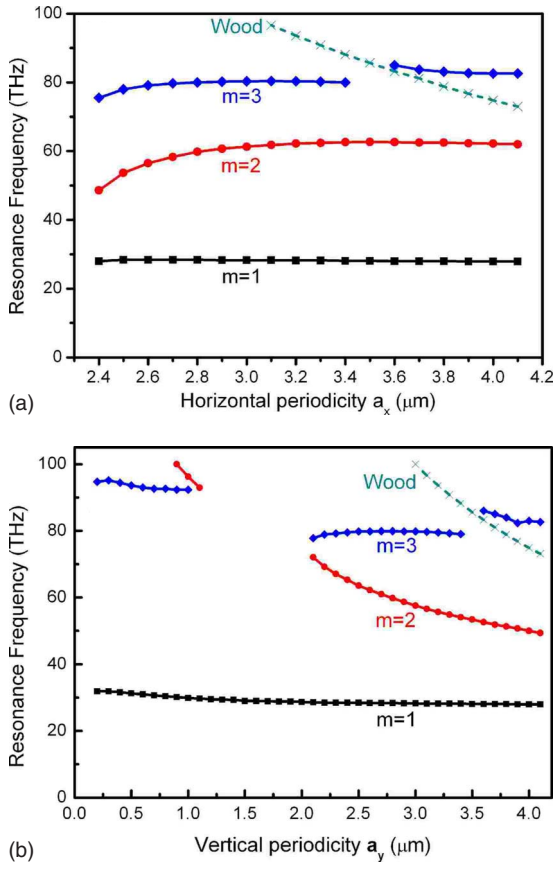

FIG. 6. (Color online) Simulation results for the resonant frequency of the first three standing-wave modes of the metamaterial shown in Fig. 1 with varying (a) horizontal (b) vertical periodicity. The frequency of the Wood anomaly is also shown. When two resonances cross each other in frequency and form a single dip, the graph does not show their spectral position as the individual resonances cannot be resolved.

4. Insertion of dielectric material between the arms

By inserting a dielectric in the space between the two arms we found that the magnetic resonances (first and third modes), which have a high electric field energy density in the space filled by the dielectric, shift down in frequency, while the electric resonance (second mode) which has a low electric field energy density in the dielectric remains unchanged. The simulated results are shown on Fig. 5(d). The third resonance can be lowered in frequency toward the second resonance. As indicated later in this paper, this tuning of the third resonance can be used as a means of achieving a negative index of refraction.

5. Changes in periodicity and far-field interactions

Figure 6 shows the effect of varying x and y periodicity of the metamaterial on the SPP resonances. It is known that the periodicity of an array of nanoparticles can shift the SPP resonance frequency and behavior (lifetime and spectral width) both due to near-field coupling[36] (on nanoparticles nearly touching) and far-field coupling. Far-field coupling dominates for distances between nanoparticles greater than a few tens of nm, and was studied in full detail theoretically in Ref. 37 and measured experimentally in Ref. 38.

For small periodicities a_x with particles nearly touching on the x direction, the second resonance shifts down in frequency due to near-field coupling (at the limit of touching nanoparticles, the metamaterial would resemble an array of infinite nanowires, which would behave as an effective plasma medium,[39] where the second resonance would move down to zero frequency). For small vertical periodicities a_y (with particles nearly touching in the y direction), the second resonance strongly shifts up in frequency disappearing even above the third resonance, the reason for this is not clear. As the periodicity is increased, the effects of far-field coupling come into play. Far-field interaction of nanoparticles can be decomposed into two problems: the dynamic depolarization of a single particle and the dipolar interaction between point dipoles.[37] In our case, only the second plasmon standing-wave resonance shows strong net dipolar moment in the XY plane, so only this resonance shows significant dipolar interaction. This explains why the LC resonance frequency does not depend in periodicity due to the lack of a net electric-dipole moment.

Figure 6 also shows the Wood anomaly. Theory predicts[37] that the dipolar interactions for a given plasmon resonance exhibit strong variations (frequency-shift and increased damping due to radiative losses) when the periodicity allows a grating order to change from evanescent ($a<a_c$, where a_c is the critical grating constant) to radiative in character ($a>a_c$). On Figs. 6(a) and 6(b) an example of such change occurs when the Wood anomaly crosses the third resonance. The increased losses are seen in the transmission spectrum (not shown) as a weaker dip with increased spectral width. The frequency shift is clearly observed.

C. Negative index of refraction

Considering only the metamaterial as seen in Fig. 1, without requiring additional wires or particles, we could achieve a simultaneous negative permittivity and permeability when the third resonance occurred just above the second one, and so obtain a LHM.

1. Downshift of the third resonance through insertion of a dielectric between the arms

Figure 7(a) shows the simulated transmission and reflection spectrum of the U-shaped nanowire with a dielectric of index $n=1.8$ inserted between both arms, and the retrieved effective parameters. The radius of the nanowire has been increased to achieve a stronger magnetic resonance. It can be seen that the third resonance has shifted down in frequency toward the second one, in agreement with Fig. 5(d), therefore achieving a simultaneously negative $\mathrm{Re}(\varepsilon_{\mathrm{eff}})$ and $\mathrm{Re}(\mu_{\mathrm{eff}})$, and thus a negative $\mathrm{Re}(n_{\mathrm{eff}})$ at a frequency of 70 THz.

We noticed that if the third resonance comes too close to the second one, for a frequency separation below a certain threshold value, a drastic change in the phase of the transmittance (not shown) takes place, and the retrieved permeability and permittivity change from being both negative to being positive, but a transmission peak where we had negative effective index is still observed due to the impedance

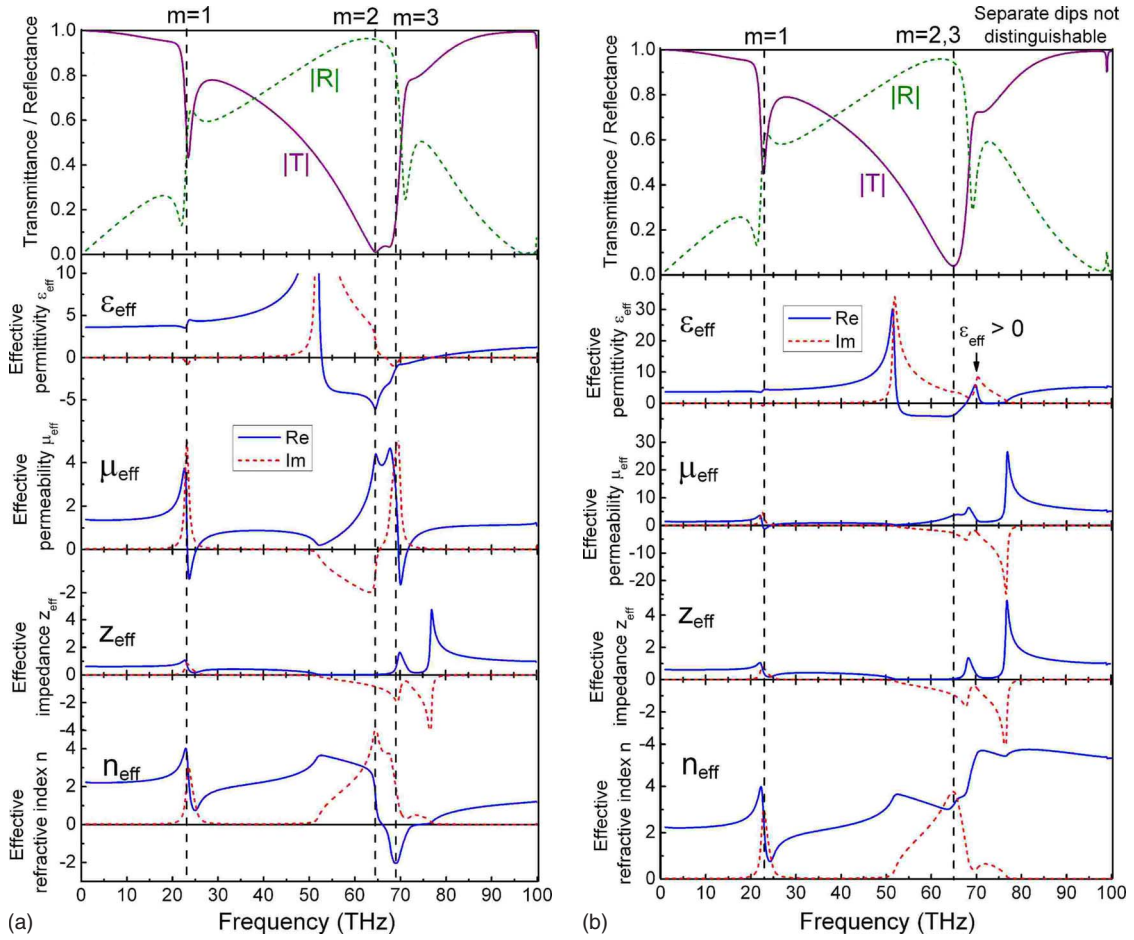

FIG. 7. (Color online) Transmittance and reflectance spectra and retrieved electromagnetic parameters of the analyzed metamaterial upon plane-wave excitation as shown in Fig. 1 when a dielectric with refractive index (a) 1.8 (b) 1.9 is introduced between the arms. Geometrical parameters are $r=150$ nm, $d=450$ nm, $L=2125$ nm, $L_{\text{tot}}=4700$ nm, $a_x=a_y=2800$ nm. On the first case (a) a negative index of refraction is retrieved. On the second case (b), both resonances are too close together and disturb each other.

approaching unity near the resonance. To achieve a negative index of refraction, we need the third resonance close to the second one, but not *too* close. As a rule of thumb we found that it is important that the two resonances show clearly distinguishable dips in the spectrum and do not merge to form a single dip. When the two dips are no longer distinguishable, no negative $\text{Re}(n_{\text{eff}})$ is retrieved. We believe that this is because when the two resonances coincide in frequency, the structure cannot support the two different field and current distributions simultaneously showing both electric and magnetic dipolar moments. We have found this criterion to be valid on all subsequent simulations. This is seen in Fig. 7(b), where a slightly higher dielectric than that on Fig. 7(a) was used: although a very slight variation in the absolute value of the transmittance spectra is seen, the two dips $m=2$ and $m=3$ merge into a single one, and drastic changes happen in the retrieved parameters resulting in a non-negative $\text{Re}(n_{\text{eff}})$.

2. Shift up of the second resonance by far-field dipolar coupling

Figure 8 shows the simulated transmission and reflection spectrum of the U-shaped nanowire with an appropriately chosen a_y periodicity [in agreement with Fig. 6(b)] that raises the frequency of the second mode closely below the third one (but not too close), so that a negative $\text{Re}(n_{\text{eff}})$ at a frequency of 80 THz is achieved.

D. Stack of several layers of metamaterial

We simulated the stacking of N layers of the metamaterial with a period a_z in the z direction. We found that the peaks seen on the single layer which could be associated with the first, second, and third slow-SPP standing-wave resonances separate into N peaks each. These N peaks associated with each resonant mode are similar to the N discrete normal modes supported by a nanoparticle chain.[40] For simplicity in explanations we use the mode nomenclature m_n, where m indicates the resonance order of the slow-SPP standing wave as used in a single layer, and $n=1\ldots N$ indicates the order of the normal mode along the z propagation direction, related with the relative phases of the mode at each layer. All the modes $m_{1\ldots N}$ show the same m-mode resonance in each nanoparticle, but with different phases between the nanoparticles in each of the N layers. Increasing the period a_z causes the $m_{1\ldots N}$ modes to move closer in frequency, and at $a_z \to \infty$ the modes become degenerate to form a single mode m,

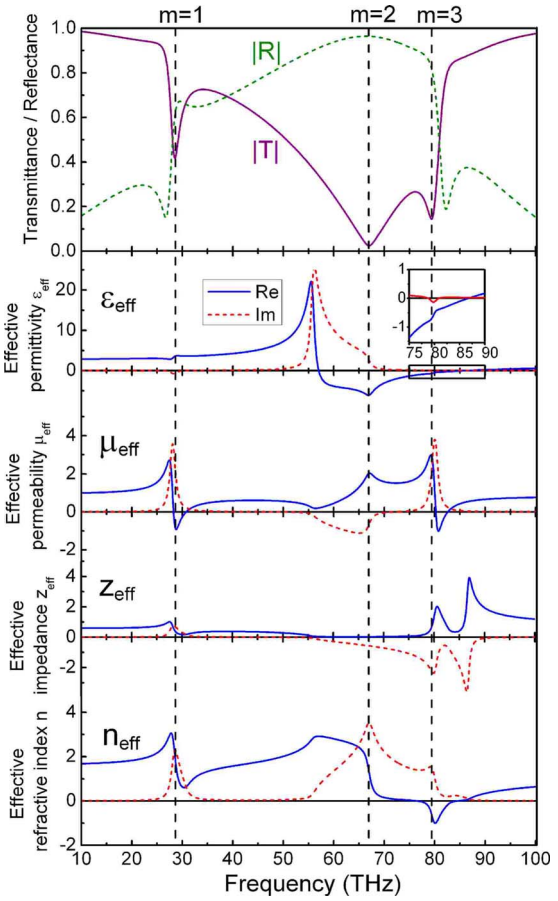

FIG. 8. (Color online) Transmittance and reflectance spectra and retrieved electromagnetic parameters of the analyzed metamaterial upon plane-wave excitation as shown in Fig. 1 with geometrical parameters $r=100$ nm, $d=450$ nm, $L=2125$ nm, $L_{\mathrm{tot}}=4700$ nm, $a_x=2800$ nm, $a_y=2300$ nm. A negative index of refraction is retrieved.

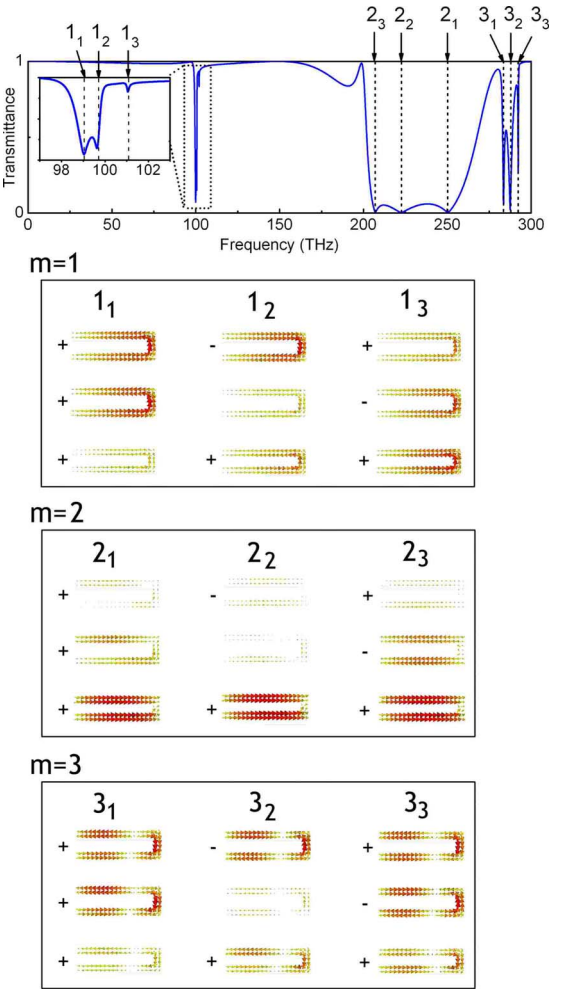

FIG. 9. (Color online) Transmission and reflection spectra for three layers of metamaterial with geometrical parameters $L=375$ nm, $h=25$ nm, $w=40$ nm, $d=50$ nm, $a_x=a_y=600$ nm, $a_z=250$ nm. For each resonance the current distributions on the three U-shaped nanostrips of a unit cell as seen from above are depicted. The incident plane wave is incident upward from the bottom in the representations. A plus or minus sign is added to each layer to indicate the phase of the electric current in that layer with respect to the first (the bottom) layer.

equal to that of a single layer. Also, if the number of layers is increased indefinitely $N\rightarrow\infty$, the modes $m_{1\ldots N}$ would form a continuous spectrum showing the true unit-cell response of the infinite medium metamaterial.

To better study this complex set of resonances, we found that reducing the loss of the metal Drude model allowed a much easier identification of resonances when stacking the metamaterial, so in this section we used in our simulations an unrealistically low-loss collision frequency of $\gamma=1\times10^{12}$ s^{-1}. This greatly reduced the resonance damping and also allowed us to easily scale down the metamaterial to work in the near infrared. Also, to simplify the meshing during simulations, a rectangular nanostrip with height h and width w was used instead of a cylindrical nanowire of radius r: the slow-SPP mode fields and dispersion relations on such nanostrips can be calculated numerically,[41] showing very similar behavior to a cylindrical nanowire.

The resonances seen on a stack of $N=3$ layers of the metamaterial are shown in Fig. 9 together with their electrical current distributions. It can be visually seen and confirmed with parameter retrieval that the new resonances $m_{1\ldots3}$ can create new VCLs or new net electric dipoles which can give the resonances $m_{1\ldots3}$ either magnetic or electric Lorentz-type responses, respectively. For example, mode 2_3 clearly shows VCLs between nanoparticles and therefore shows a magnetic response.

Similar to the case with one layer, we adjusted the geometrical parameters of the $N=3$ layered metamaterial so that the electric resonance 2_1 (which is the highest in frequency of the $m=2$ resonances) occurred at a frequency just below the magnetic resonance 3_1 (the lowest in frequency of the $m=3$ resonances), yielding a negative real part of the effective refraction index around 280 THz. Again, it was of utmost importance that both resonances where separated enough as to show distinct dips in the transmission spectrum so they were not interfering with each other. The transmission and reflection spectra and retrieved effective parameters are shown in Fig. 10.

Finally, the time-varying electromagnetic fields were simulated on the designed $N=3$ layered material at 282 THz,

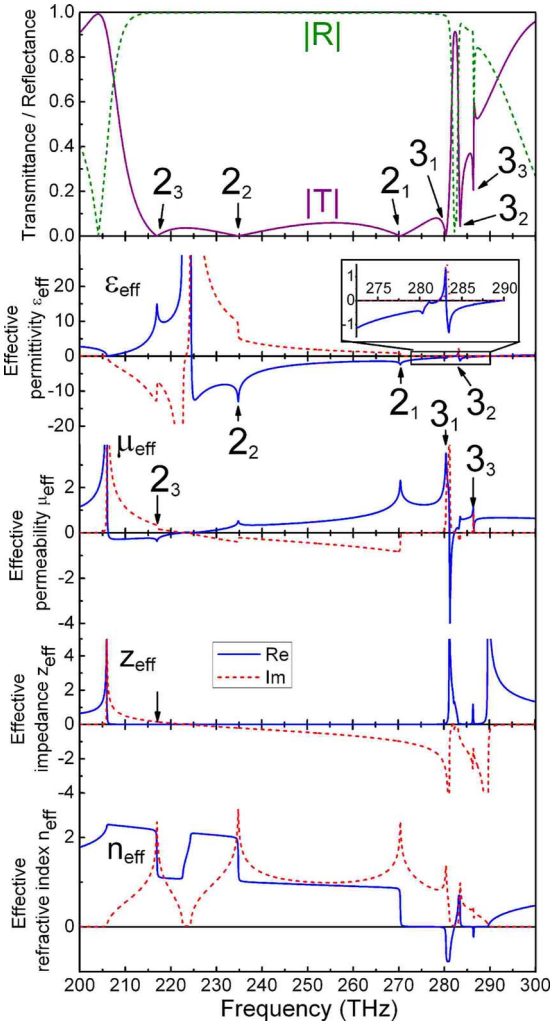

FIG. 10. (Color online) Transmission and reflection spectra, together with retrieved electromagnetic parameters for three layers of the metamaterial with geometrical parameters $L=375$ nm, $h=25$ nm, $w=40$ nm, $d=35$ nm, $a_x=600$ nm, $a_y=500$ nm, $a_z=260$ nm. On resonance 3_1, the permeability shows a Lorentz-type resonance yielding negative permeability and the effective permittivity is still negative due to the proximity of resonance 2_1, therefore a negative index of refraction is retrieved around 280 THz.

where n_{eff} was found to be negative, and the backward wave propagation inside the LHM composed only of U-shaped nanowires was clearly observed, as shown in Fig. 11. Remember that this last simulation on near infrared frequencies considered low losses: if we use experimental data[24] for gold in this case it results in weak resonances and no double-negative behavior. The losses are thus the main limitation when designing the proposed metamaterial above far-infrared frequencies, as is common in all SRR-based metamaterials.

V. CONCLUSION

In summary, we have performed simulations confirming that the nanowire slow-SPP standing-wave resonator model is very adequate to analyze the resonances in an array of

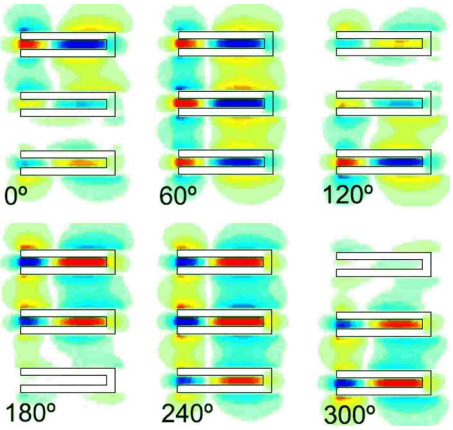

FIG. 11. (Color online) Simulated magnetic field H_y over time at 280 THz for the XZ plane of a unit cell of the metamaterial described measured in Fig. 10. The incident plane-wave propagates upward from below. Backward phase propagation can be seen inside the metamaterial.

SRRs, also called U-shaped or horseshoe-shaped nanowires. Use of the slow-SPP dispersion relation together with the standing-wave condition can be useful to predict the frequency position and behavior of the several standing-wave modes in the SRR as a function of geometrical parameters. To refine the predictions, far-field coupling between unit cells should be taken into account using the appropriate dipolar interaction model,[37] and near-field coupling between the two arms should also be taken into account when they are close together. Under certain restrictions (very thin nanowires and dimensions much shorter than the wavelength) the coupling between arms can be analyzed as the MPR between two nanowires.[35]

When the U-shaped nanowires were used as unit cell of a metamaterial, we saw through effective parameter retrieval methods how the various standing-wave resonances can show either an electric or magnetic effective response depending on their current and field distributions, thus yielding negative constitutive parameters just above the resonant frequency. We demonstrated on simulations some methods of making the third resonance (which shows a magnetic response) exist in a frequency just above the second resonance (which shows an electric response) and so achieve a negative effective refractive index in the far-infrared region of the spectrum. In contrast with typical metamaterials, negative permittivity and permeability have been obtained through different resonances on the *same* structure.

We also performed simulations on the effect of stacking the metamaterial into N layers, and described how each standing-wave resonance mode m splits into N normal-mode resonances $m_{1\ldots N}$ each showing its own electric or magnetic response. We performed simulations showing how these resonances can also be shifted adequately to achieve a LHM showing backward wave propagation.

ACKNOWLEDGMENTS

Financial support by the Spanish MCyT and EU-FEDER

under Contract No. TEC2008-06871-C02-02 is gratefully acknowledged. R.O. and C.G-M. also acknowledge financial support from the FPI grant program of Universidad Politécnica de Valencia.

*frarodfo@ntc.upv.es

[1] V. G. Veselago, Sov. Phys. Usp. **10**, 509 (1968).
[2] J. B. Pendry, Phys. Rev. Lett. **85**, 3966 (2000).
[3] R. A. Shelby, D. R. Smith, and S. Schultz, Science **292**, 77 (2001).
[4] T. J. Yen, W. J. Padilla, N. Fang, D. C. Vier, D. R. Smith, J. B. Pendry, D. N. Basov, and X. Zhang, Science **303**, 1494 (2004).
[5] C. Enkrich, M. Wegener, S. Linden, S. Burger, L. Zschiedrich, F. Schmidt, J. F. Zhou, Th. Koschny, and C. M. Soukoulis, Phys. Rev. Lett. **95**, 203901 (2005).
[6] V. Yannopapas and N. V. Vitanov, Phys. Rev. B **74**, 193304 (2006).
[7] C. Rockstuhl, F. Lederer, C. Etrich, T. Pertsch, and T. Scharf, Phys. Rev. Lett. **99**, 017401 (2007).
[8] J. Zhou, Th. Koschny, M. Kafesaki, E. N. Economou, J. B. Pendry, and C. M. Soukoulis, Phys. Rev. Lett. **95**, 223902 (2005).
[9] C. Rockstuhl, F. Lederer, C. Etrich, Th. Zentgraf, J. Kuhl, and H. Giessen, Opt. Express **14**, 8827 (2006).
[10] C. Rockstuhl, T. Zentgraf, E. Pshenay-Severin, J. Petschulat, A. Chipouline, J. Kuhl, T. Pertsch, H. Giessen, and F. Lederer, Opt. Express **15**, 8871 (2007).
[11] R. H. Ritchie, Phys. Rev. **106**, 874 (1957).
[12] C. A. Pfeiffer, E. N. Economou, and K. L. Ngai, Phys. Rev. B **10**, 3038 (1974).
[13] J. C. Ashley and L. C. Emerson, Surf. Sci. **41**, 615 (1974).
[14] J. Takahara, S. Yamagishi, H. Taki, A. Morimoto, and T. Kobayashi, Opt. Lett. **22**, 475 (1997).
[15] T. Søndergaard and S. Bozhevolnyi, Phys. Rev. B **75**, 073402 (2007).
[16] S. I. Bozhevolnyi and T. Søndergaard, Opt. Express **15**, 10869 (2007).
[17] H. Ditlbacher, A. Hohenau, D. Wagner, U. Kreibig, M. Rogers, F. Hofer, F. R. Aussenegg, and J. R. Krenn, Phys. Rev. Lett. **95**, 257403 (2005).
[18] E. K. Payne, K. L. Shuford, S. Park, G. C. Schatz, and C. A. Mirkin, J. Phys. Chem. B **110**, 2150 (2006).
[19] T. Søndergaard and S. Bozhevolnyi, Opt. Express **15**, 4198 (2007).
[20] G. Della Valle, T. Søndergaard, and S. I. Bozhevolnyi, Opt. Express **16**, 6867 (2008).
[21] V. A. Podolskiy, A. K. Sarychev, and V. M. Shalaev, J. Nonlinear Opt. Phys. Mater. **11**, 65 (2002).
[22] V. Yannopapas, Phys. Status Solidi (RRL) **1**, 208 (2007).
[23] V. Yannopapas, J. Phys.: Condens. Matter **20**, 255201 (2008).
[24] P. B. Johnson and R. W. Christy, Phys. Rev. B **6**, 4370 (1972).
[25] G. Schider, J. R. Krenn, A. Hohenau, H. Ditlbacher, A. Leitner, F. R. Aussenegg, W. L. Schaich, I. Puscasu, B. Monacelli, and G. Boreman, Phys. Rev. B **68**, 155427 (2003).
[26] Jiunn-Woei Liaw and Po-Tsang Wu, Opt. Express **16**, 4945 (2008).
[27] J. B. Pendry, A. J. Holden, D. J. Robbins, and W. J. Stewart, IEEE Trans. Microwave Theory Tech. **47**, 2075 (1999).
[28] D. J. Cho, F. Wang, X. Zhang, and Y. R. Shen, Phys. Rev. B **78**, 121101(R) (2008).
[29] R. W. Wood, Philos. Mag. **4**, 396 (1902).
[30] R. W. Wood, Phys. Rev. **48**, 928 (1935).
[31] D. R. Smith, D. C. Vier, Th. Koschny, and C. M. Soukoulis, Phys. Rev. E **71**, 036617 (2005).
[32] D. R. Smith, S. Schultz, P. Markos, and C. M. Soukoulis, Phys. Rev. B **65**, 195104 (2002).
[33] X. Chen, T. M. Grzegorczyk, B.-I. Wu, J. Pacheco, Jr., and J. Au Kong, Phys. Rev. E **70**, 016608 (2004).
[34] T. Koschny, P. Markos, D. R. Smith, and C. M. Soukoulis, Phys. Rev. E **68**, 065602(R) (2003).
[35] A. K. Sarychev, G. Shvets, and V. M. Shalaev, Phys. Rev. E **73**, 036609 (2006).
[36] M. Quinten, A. Leitner, J. R. Krenn, and F. R. Aussenegg, Opt. Lett. **23**, 1331 (1998).
[37] M. Meier, A. Wokaun, and P. F. Liao, J. Opt. Soc. Am. B **2**, 931 (1985).
[38] B. Lamprecht, G. Schider, R. T. Lechner, H. Ditlbacher, J. R. Krenn, A. Leitner, and F. R. Aussenegg, Phys. Rev. Lett. **84**, 4721 (2000).
[39] J. B. Pendry, A. J. Holden, W. J. Stewart, and I. Youngs, Phys. Rev. Lett. **76**, 4773 (1996).
[40] W. H. Weber and G. W. Ford, Phys. Rev. B **70**, 125429 (2004).
[41] P. Berini, Opt. Lett. **24**, 1011 (1999).